Tectonophysics 762 (2019) 97–108

Contents lists available at ScienceDirect

Tectonophysics

journal homepage: www.elsevier.com/locate/tecto

The Pucallpa Nest and its constraints on the geometry of the Peruvian Flat Slab

Lara S. Wagner[a,*], Emile A. Okal[b]

[a] Department of Terrestrial Magnetism, Carnegie Institution for Science, 5241 Broad Branch Rd NW, Washington, DC 20015, USA
[b] Department of Earth & Planetary Sciences, Northwestern University, Evanston, IL 60208, USA

ARTICLE INFO

Keywords:
Seismic nest
Intermediate-depth seismicity
Peru
Flat-slab subduction

ABSTRACT

Seismic nests (or clusters) are typically defined as regions of high seismic activity at intermediate depths that do not move over time and are not associated with volcanic activity at the surface (e.g. Zarifi and Havskov, 2003; Zarifi et al., 2007; Prieto et al., 2012). In this study, we focus on a seismic nest located in central Peru beneath the Amazon basin city of Pucallpa. The location of this nest is just beyond the eastern-most extent of the Peruvian flat slab, similar to the settings of two other South American clusters, the Bucaramanga and Pipanaco nests. While the Pucallpa nest is visible in the figures of many earlier papers on intermediate depth South American seismicity, it has not to our knowledge been described as a seismic nest before. We present the first detailed description of the Pucallpa nest, compare it to other established nests, and discuss its implications for our understanding of the Peruvian flat slab. Our results indicate that the Pucallpa nest demarcates the northern margin of a sag in the horizontally subducting Nazca plate in central Peru. The position of the nest along the projected location of the downgoing Mendaña fracture zone is consistent with local variations in b-values and could help to explain both the nest's genesis and the co-located change in slab geometry. The nest is also spatially well correlated with the northern margin of the thick-skinned Shira Mountains and with the high heat flow associated with the Agua Caliente dome (Hermoza et al., 2006; Navarro Comet, 2018). Further study is needed to understand the effects of the complex Peruvian slab geometry on the formation of thick skinned deformation and heat flow anomalies on the overriding South American continent.

1. Introduction and tectonic setting

The Pucallpa seismic nest is located in eastern central Peru, near the border with Brazil. It is visible to first order as a cluster of intermediate depth earthquakes (140–180 km) that are located ~200 km east of the Andean orogen in a region otherwise characterized by very low rates of sub-Moho seismicity. While there is no official definition for what comprises a seismic nest, there is some general consensus in the literature that nests should meet the following criteria: 1) the seismicity occurs within a relatively confined volume, 2) the amount of seismicity within that volume is significantly higher than in surrounding regions, 3) the location of the nest must be stationary and not time-dependent, and 4) the nest is not associated with overriding volcanism (e.g. Zarifi and Havskov, 2003; Prieto et al., 2012). Some of the best studied nests include the Bucaramanga nest in Colombia, the Vrancea nest in Romania, and the Hindu Kush nest in Afghanistan. Other nests/clusters have been described that match most if not all of the aforementioned criteria, including the Socompa nest in northern Argentina (Sacks et al., 1966), the Fiji nest (Isacks et al., 1967; Schneider et al., 1987; Zarifi and Havskov, 2003), the Ecuador nest (Zarifi and Havskov, 2003), the Cauca cluster in central Colombia (Chang et al., 2017), and the Pipanaco nest in central Argentina (Cahill and Isacks, 1992; Mulcahy et al., 2014).

The causes of seismic nests are not well constrained. Intermediate depth seismicity is often associated with the dehydration of downgoing oceanic slabs (e.g. Green and Houston, 1995; Hacker et al., 2003; Okazaki and Hirth, 2016) or with self-localized shear-heating along existing fault planes in the subducted plate (e.g. Kelemen and Hirth, 2007; John et al., 2009; Prieto et al., 2013; Poli et al., 2016). As is the case along most of the Peruvian margin, the subducting Nazca plate near Pucallpa descends normally to approximately 70–100 km depth and then flattens, traveling horizontally for over 400 km before resuming its descent into the mantle. This unusual “flat slab” geometry results in the presence of relatively shallow intermediate depth seismicity well east of where normal Wadati-Benioff zone seismicity would usually be expected. The detailed geometry of the downgoing Nazca

* Corresponding author.
E-mail address: lwagner@carnegiescience.edu (L.S. Wagner).

https://doi.org/10.1016/j.tecto.2019.04.021
Received 17 October 2018; Received in revised form 9 April 2019; Accepted 20 April 2019
Available online 23 April 2019
0040-1951/

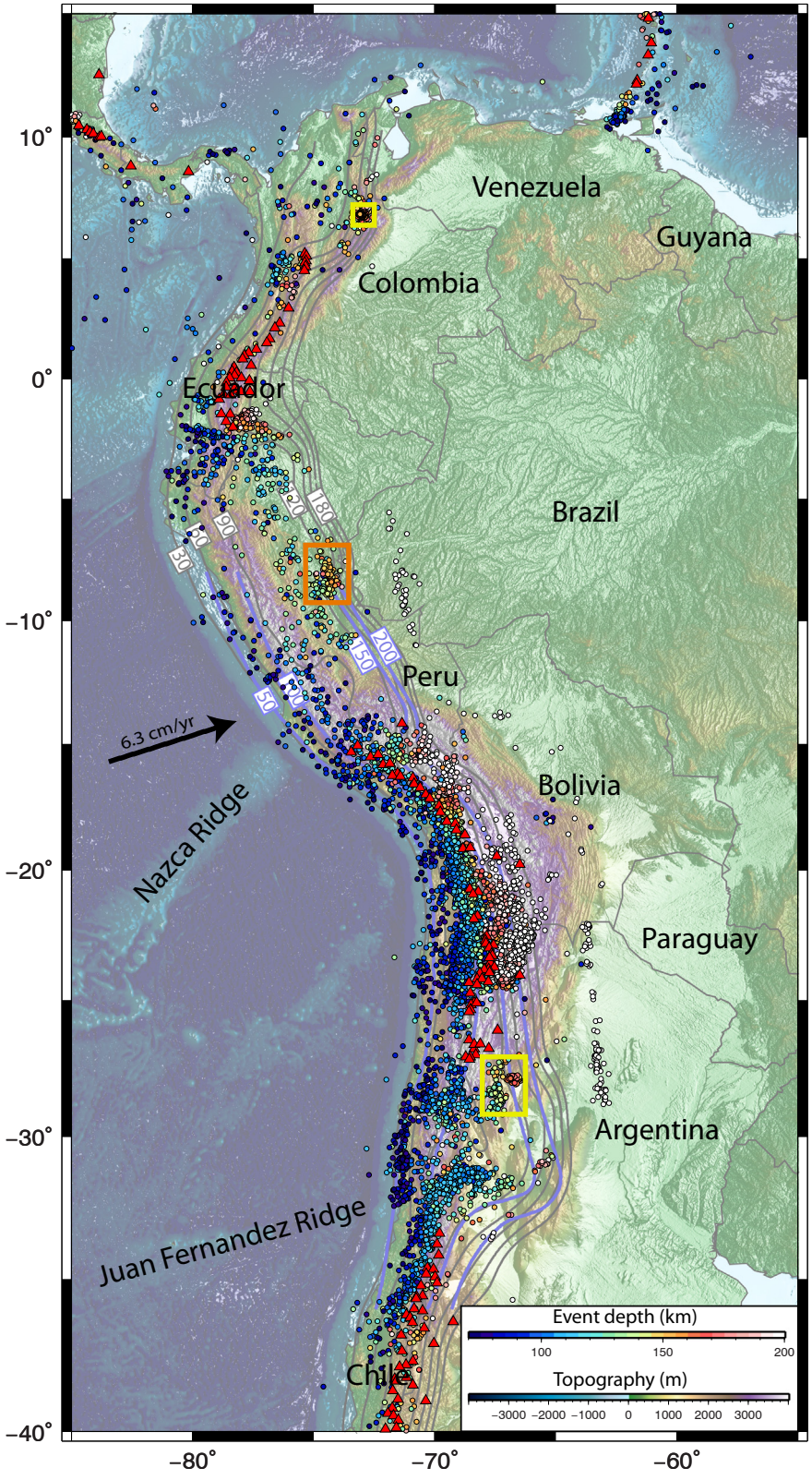

Fig. 1. Map of South American seismicity and Holocene volcanism. Red triangles indicate Holocene volcanism from the Global Volcanism Project (2013). Circles indicate earthquakes from Jan 1990 to Jan 2015 listed in the Reviewed International Seismological Centre On-line Bulletin (2015) with magnitudes > 4 and depths > 70 km. Orange box shows Pucallpa nest described in this study. Yellow boxes show other nests: the Bucaramanga nest in Colombia and the Pipanaco nest in Argentina. The faded black lines show slab contours from Slab 2.0 (Hayes et al., 2018). The faded blue lines show slab contours from Cahill and Isacks (1992). The black arrow offshore shows relative Nazca-South America plate motion from Altamimi et al. (2016). (For interpretation of the references to color in this figure legend, the reader is referred to the web version of this article.)

plate near Pucallpa has been poorly constrained in part due to the lack of publicly available seismic data from the region. Existing models generally suggest that the nest lies along or just beyond the easternmost extent of the Peruvian flat slab (e.g. Cahill and Isacks, 1992; Gutscher et al., 2000; Hayes et al., 2018) (Figs. 1 and 2). This is similar to the locations of two other South American seismic nests, the Bucaramanga nest in Colombia and the Pipanaco nest in Argentina, both of which are located in the portion of the downgoing plate that has resumed normal subduction beyond a flat slab segment (Fig. 1).

The causes of flat slab subduction, both in Peru and elsewhere, are still a topic of ongoing research. Possible contributing factors include the age of the subducting plate, the relative convergence rates of the

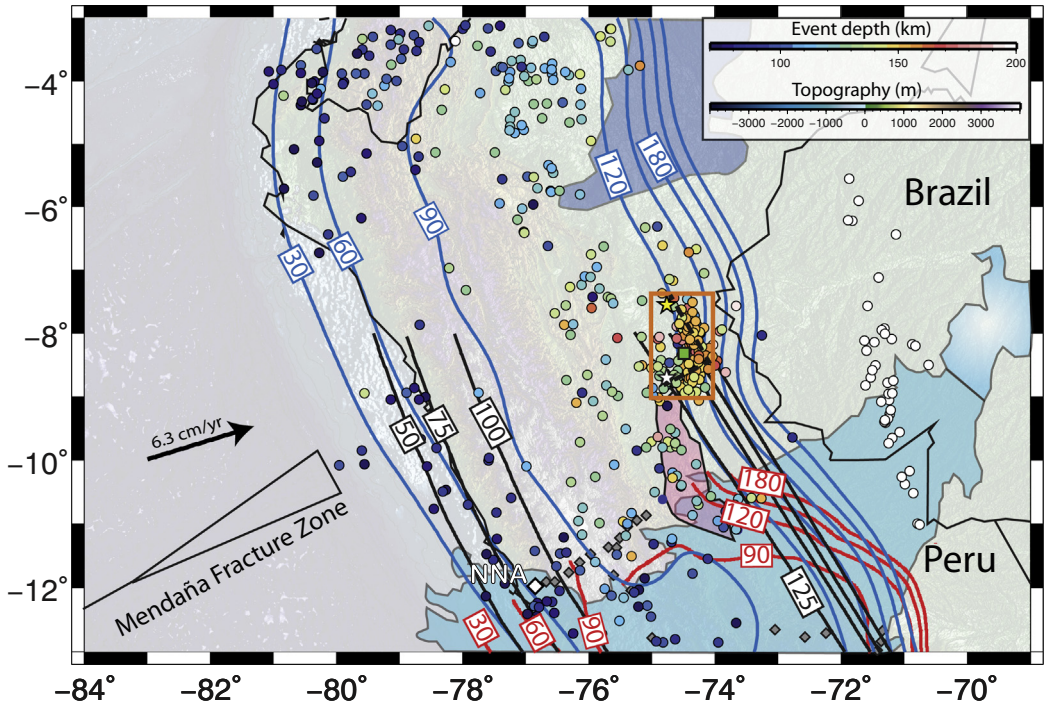

Fig. 2. Map of Pucallpa Nest. Circles indicate earthquakes as plotted in Fig. 1. The orange box shows the Pucallpa nest described in this study. The black dashed line indicates NNW and WSW legs of the Pucallpa Nest. The green square is the location of the city of Pucallpa. The yellow star indicates the location of the 2011 M_w = 7.0 Contamana earthquake (Tavera, 2012) located at 148 km depth. The white star indicates the location of the Agua Caliente Oil Field and Boiling River (Hermoza et al., 2006; Ruzo, 2016; Navarro Comet, 2018). Offshore black lines show the outline of the Mendaña fracture zone from Huchon and Bourgois (1990). Light blue outlined shape is the projected location of the subducted Nazca Ridge based on its conjugate Tuamotu Plateau on the Pacific plate (Hampel, 2002). The dark blue outlined shape is the subducted Inca Plateau based on the location of its conjugate, the Marquesas Plateau (Rosenbaum et al., 2005). The pink shaded region shows the location of the Shira Mountains (Hermoza et al., 2006). The nearest permanent seismic station (NNA) is shown as a white diamond. PULSE seismic stations are shown as small grey diamonds. The blue lines show slab contours from Slab 2.0 (Hayes et al., 2018) in 30 km depth intervals. The black lines show slab contours from Cahill and Isacks (1992) in 25 km intervals. The red lines show approximate slab contours from the PULSE deployment (Antonijevic et al., 2015; Scire et al., 2016; Bishop et al., 2017) in 30 km intervals. (For interpretation of the references to color in this figure legend, the reader is referred to the web version of this article.)

oceanic and continental plates, the extent of trench rollback or continental advance, the thickness of the continental mantle lithosphere particularly in the case of a cratonic root, and the presence of overthickened oceanic crust due to a hotspot track or oceanic plateau that could add buoyancy to the descending slab (e.g. Gerya et al., 2009; Manea et al., 2012; O'Driscoll et al., 2012; Antonijevic et al., 2015). In South America, both the Chilean and the southern portion of the Peruvian flat slabs show close spatial alignments between the shallowest portions of the flat slabs and downgoing seamount chains, the Juan Fernandez and Nazca Ridges respectively (e.g. Anderson et al., 2007; Antonijevic et al., 2015, 2016). The timing of the arrival of these ridges also closely aligns with the formation of ore deposits and the cessation of arc volcanism in both Peru and Chile/Argentina (Kay and Mpodozis, 2001; Yáñez et al., 2001; Hampel, 2002; Rosenbaum et al., 2005). This suggests that, while other factors almost certainly play a role (i.e. trench rollback, presence of cratonic roots), the buoyancy of downgoing slabs seems to have a strong effect on the geometry of flat slabs, and appears to be a necessary (if not sufficient) contributing factor for their formation.

Most of the Peruvian flat slab lies north of the Nazca Ridge, raising the question of why this flat slab region is so broad if the Nazca Ridge is necessary for its formation. The southern half of the Peruvian flat slab can be accounted for by the southward migration of the Nazca Ridge relative to the overriding plate over time due to the difference between the trend of the ridge track and the plate convergence directions (e.g. Hampel, 2002; Rosenbaum et al., 2005; Antonijevic et al., 2015). The northern portion of the Peruvian flat slab, however, must have an independent explanation. Gutscher et al. (1999, 2000) proposed that the northern portion of the Peruvian flat slab was supported by the completely subducted Inca Plateau, the conjugate of the Marquesas Plateau on the Pacific plate. In between the subducted Inca plateau and the downgoing Nazca Ridge, they proposed a sag in the downgoing plate whose deepest portion aligns with the subducting Mendaña Fracture Zone (MFZ) (Gutscher et al., 1999, 2000; Huchon and Bourgois, 1990; Lonsdale, 2005). The Pucallpa Nest lies approximately along the projected location of the MFZ.

At the surface, the Peruvian flat slab is characterized by a gap in Holocene volcanism between 2°S and 14°S. The nearest Holocene volcanism to the Pucallpa nest lies over 700 km to the south or over 800 km to the northwest. While there is no known volcanism above the Pucallpa nest, there is evidence for high heat flow in the form of boiling rivers associated with the recent rapid uplift of the Agua Caliente dome (Hermoza et al., 2006; Ruzo, 2016; Navarro Comet, 2018). This small dome and associated boiling rivers lies at the northern end of the thick-skinned Shira Mountains (Fig. 2) (James and Snoke, 1994; Hermoza et al., 2006). The uplift of the Shira Mountains and adjacent Agua Caliente dome occurred due to the inversion of Paleozoic extensional structures at 7.2–5.3 Ma, resulting in thick skinned deformation along the ~20–25 km deep Shira Mountain fault (Hermoza et al., 2006; Alvarez, 2008; Espurt et al., 2008). This timing corresponds to the time of formation of zinc and copper ore deposits and the cessation of arc volcanism at these latitudes (e.g. Rosenbaum et al., 2005).

2. The Pucallpa Nest – by the numbers

For this study, we use event locations from the International Seismic

Centre Reviewed Seismic Catalog (RISC). The nearest permanent seismic station to the Pucallpa nest is NNA, located over 450 km to the southwest. The nearest broadband seismic station with data available at the Incorporated Research Institutions for Seismology Data Management Center (IRIS-DMC) is the northernmost station for the PerU Lithosphere and Slab Experiment (Wagner et al., 2010) located ~270 km south of the Pucallpa Nest. For consistency, we use the same RISC event catalog when comparing the Pucallpa Nest to other clusters, even when other clusters have published seismicity studies based on more regional data sets. For the Pucallpa Nest, we find a relatively tight cluster of events that is most pronounced between 7.5°S and 9°S, 75°W and 74°W, and between 140 and 180 km depth (Fig. 2). The cluster roughly comprises two legs forming a backwards "L" geometry – a longer one that trends NNW and includes seismicity over the full depth range of the cluster, and a second, shorter leg extending WSW from the southern end of the NNW trending leg that includes little seismicity deeper than 160 km depth.

In the absence of openly available data from regional networks, the resulting locations could show a systematic bias. However, this should not, in principle, affect the *relative* location of regional seismicity, and hence the definition of a cluster. To test further the robustness of the locations we used, we considered a sub-dataset of 150 earthquakes, and compared the hypocentral estimates reported by the RISC and the International Data Center (IDC) operated by the Comprehensive Test Ban Treaty Organization (CTBTO). These two agencies systematically relocate global seismicity using similar methodologies, but potentially slightly different datasets. We find that the 3-D distance separating the hypocenters is on the average 14 km, and the average absolute difference in depth only 8 km, both numbers representing only a fraction of the size of the cluster. The average horizontal displacements between the two set of epicenters were < 1 km, indicating no systematic bias between the position of two estimates of the position of the cluster.

Table 1 shows the event statistics for the Pucallpa nest in comparison to the better-studied Bucaramanga, Hindu Kush, and Vrancea nests, as well as the Pipanaco nest in Argentina. We compiled datasets from the RISC from January 1990 to January 2015, with a magnitude threshold $m_b \geq 4$, which are thus believed complete. We also consider the NEIC catalog, extending back to 1963, since shorter time windows can undersample high magnitude seismicity as in the case of the catastrophic 1977 Bucharest earthquake, part of the Vrancea nest. We also compiled all Centroid Moment Tensor (CMT) solutions available for the nests, from the GlobalCMT catalog (Dziewonski et al., 1981; Ekström et al., 2012), complemented by the dataset of intermediate-depth WWSSN-era CMTs inverted by Chen et al. (2001).

Finally, for those events postdating 1990 and with $M_0 \geq 10^{25}$ dyn∗cm, we compiled the values of the energy-to-moment parameter Θ recently obtained by Saloor and Okal (2018), which characterizes the relative distribution of moment release between high- and low-frequency parts of the spectrum, and as such is a proxy for anomalous slowness or "snappyness" expressing violation of scaling laws (Newman and Okal, 1998). For depths typical of the various nests studied here, Saloor and Okal (2018) obtained a worldwide average $< \Theta > = -4.77 \pm 0.24$, but a slightly larger value (-4.57 ± 0.22) in the Hindu Kush. Their dataset comprises five values in the Pucallpa nest: -4.48 for the large 2011 event, and -4.86 ± 0.06 for the other four, suggesting that the events in the nest are not demonstrably different in their source spectrum from their world-wide counterparts in the same depth range. Only one Θ value each is available for Bucaramanga (-4.50) and Vrancea (-4.82), suggesting similar conclusions albeit on obviously minimal datasets.

We also examined the possibility of an anomalous source behavior in the Pucallpa nest by analyzing the non-double-couple CLVD components of the 14 moment tensor solutions ($M_0 \geq 2 \times 10^{24}$ dyn∗cm; $M_w \geq 5.5$) available in the GlobalCMT catalog, as characterized by the parameter (Shuler et al., 2013)

$$\varepsilon = \frac{-\lambda_2}{\mathrm{Max}\,(|\lambda_1|, |\lambda_3|)} \quad (1)$$

where $\lambda_1 \geq \lambda_2 \geq \lambda_3$ are the principal values of the deviatoric moment tensor solution (we recall that in general $-0.5 \leq \varepsilon \leq 0.5$, and that $\varepsilon = 0$ for a pure double-couple). We find ε values ranging from -0.32 to 0.20, with an average $|\varepsilon|$ of 0.11. Worldwide values in similar depth and moment windows are $-0.43 \leq \varepsilon \leq 0.47$ and $|\varepsilon| = 0.11$. We conclude that events in the Pucallpa nest are characterized neither by systematically anomalous slowness parameters Θ nor by systematic departures of their sources from double-couples beyond those observed worldwide at similar depths.

For the Bucaramanga, Hindu Kush, and Vrancea nests, we used the depth constraints as shown in Prieto et al. (2012). For the Pipanaco nest, significantly fewer studies exist that describe its geometry with the level of detail available for the aforementioned three. The Pipanaco nest demarcates the southern margin of a region of sparse intermediate depth seismicity sometimes referred to as the Antofalla teleseismic gap (Cahill and Isacks, 1992; Mulcahy et al., 2014). This seismic gap, along

Table 1
Earthquake statistics for the Pucallpa and other seismic nests.

	Pucallpa	Pipanaco (all)	Pipanaco (2)	Bucaramanga	Hindu Kush	Vrancea
Latitude range (°N)	−9.0, −7.5	−29.0, −27.4	−28.1, −27.7	6.7, 6.9	35.5, 38.5	45.3, 45.9
Longitude range (°E)	−75.0, −74.0	−67.8, −66.4	−67.0, −66.4	−73.2, −72.9	69.3, 74.5	26.1, 26.9
Depth range (km)	140–180	110–180	140–180	145–165	70–250	70–170
Approx. volume (km^3)	735,000	1.72×10^6	70,000	15,000	12.5×10^6	416,000
M > 4 (1990–2015)	105	154	72	234	1537	220
… per 1000 km^3	0.14	0.11	1.0	15.9	0.12	0.53
M > 3 (1963–2015)	245	361	170	691	5284	346
b-Values						
This study	1.02 0.90 (NNW); 1.29 (WSW)	1.67	1.44	1.70	1.23	0.88–1.14
Prieto et al. (2012)				1.35–1.6	1.15	1.15
Frohlich and Nakamura (2009)				1.59		
Zarifi and Havskov (2003)				1.17	1.43	1.00
GCMT solutions (1976–2018)	28	27	14	35	259	24
$M_0 > 2 \times 10^{24}$ dyn∗cm	12	6	4	4	106	7
(1962–1975) Chen et al. (2001)	1	1	1	1	7	0
Largest event (1976–2018)	24 Aug 2011	10 Jun 1985	25 May 1999	10 Mar 2015	26 Oct 2015	04 Mar 1977
M_0 (dyn∗cm)	4.3×10^{26}	4.0×10^{25}	5.4×10^{24}	3.0×10^{25}	2.2×10^{27}	2.0×10^{27}
Fatalities (known)					400	1500
Θ (largest event post-1990) (Saloor and Okal, 2018)	−4.48			−4.50	−4.05	−4.82 (31 May 1990)
Largest event (1962–1975; WWSSN)				29 Jul 1967		
M_0 (dyn∗cm)				1.8×10^{26}		

with the northern portion of the Pipanaco nest, was recently studied by a series of broadband and intermediate period seismic deployments (see Mulcahy et al., 2014). They combined their local data with teleseismic data to look at detailed event distributions and found the Pipanaco nest to be comprised of three separate sub-clusters. Of these, according to the RISC, the cluster furthest to the east (cluster #2, Mulcahy et al., 2014) is by far the most dense. It is also the furthest from the volcanic arc that lies west of all three sub-nests.

Note that the comparisons proposed in Table 1 and discussed below could be marred by undersampling, as exemplified by the fact that the largest known event in the Bucaramanga nest occurred in 1967, before the era of digital seismology, and was revealed as such only through the catalog of Chen et al. (2001). This remark notwithstanding, most of the nests examined in Table 1 feature some unique property. The Hindu Kush cluster is clearly in a class by itself, in terms of total volume, number of events and recurrence of large shocks (2015, 1965, and, incidentally, probably also 1909). Note, however, that the Vrancea nest comes in as a close second in terms of maximum moment; given its more shallow character, it is the most lethal nest, having resulted in catastrophic earthquakes claiming > 1000 lives in 1940 and 1977, with a long string of historical destructive events, such as the potentially larger 1802 earthquake (Georgescu, 2002). The Bucaramanga nest clearly features the densest seismicity per unit volume, at a level ($m_b \geq 4$) where completeness can reasonably be assumed, at least since 1990.

As for the Pucallpa Nest, it is larger in volume than all but the Hindu Kush and combined Pipanaco clusters, but is similar to the Vrancea nest. The seismic rate is somewhat lower than for several other nests, though this may be due to an underreporting of events because of the relative lack of local seismic data. What makes the seismicity in the Pucallpa nest notable is its location in a region that is otherwise almost devoid of seismicity (Figs. 2, 3). Other nests like Bucaramanga, while far more active than the Pucallpa nest, are also located within clearly observed and relatively active Wadati-Benioff Zones. Between 1990 and 2015, the Pucallpa nest produced somewhere between 1 and 15 events each year that are compiled in the RISC (Fig. 4). The average number of

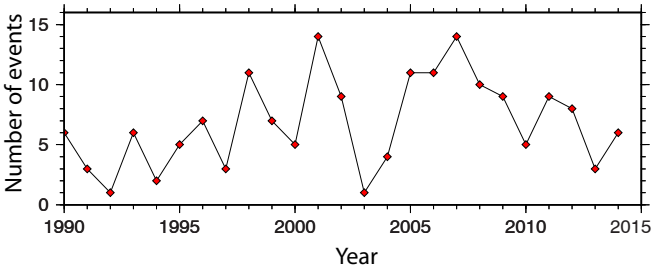

Fig. 4. Number of events per year. Number of events of any magnitude between 1990 and 2015 from the Reviewed ISC On-line Bulletin (2015) within the Pucallpa Nest (between 7.6°S and 9°S latitude, between 74°W and 75°W longitude, and between 130 and 180 km depth).

events per year in that time window was 6.8 with a standard deviation of 3.7. There is no indication that the seismicity in this cluster has moved spatially during this 25-year time window. The largest event during our study time window in the Pucallpa nest is the 24 August 2011 Contamana earthquake (RISC $m_b = 6.6$; $M_w = 7.0$ (Tavera, 2012)). The location of this earthquake lies at the northern edge of the Pucallpa Nest, at the end of the longer NNW-SSE trending leg. This event produced 35 aftershocks with magnitudes between 3.5 and 5.0 (Tavera, 2012), though only one was recorded at sufficient numbers of stations to determine a location. The fact that the largest event occurs at the edge of the group is reminiscent of the observation, on a much larger scale, that the largest intermediate and deep earthquakes tend to occur at the bottom or at the lateral edges of groups of deep seismicity (Kirby et al., 1996, Fig. 21).

2.1. Frequency-magnitude relationships

We next analyze the frequency-magnitude relations in the various nests, with the results shown on Fig. 5, and listed as *b*-values in Table 1, where they are compared with those of previous studies when available. Following Rundle (1989), we recall that, under the assumption of

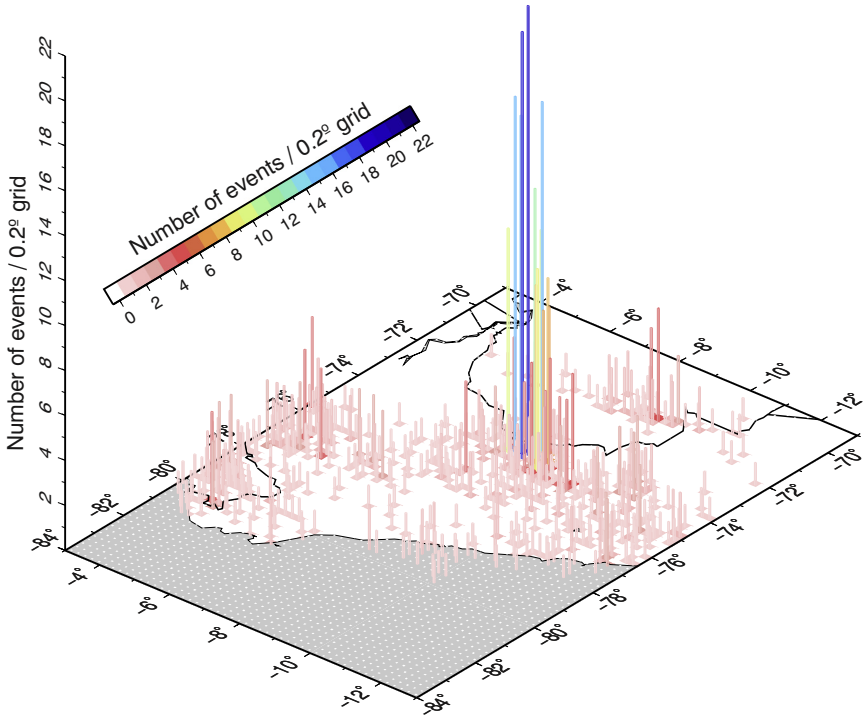

Fig. 3. Histogram of the number of events. Included are events of depth > 70 km of any magnitude between 1990 and 2015 from the Reviewed ISC On-line Bulletin (2015) per 0.2° × 0.2° grid in map view. The Pucallpa cluster is clearly visible as having substantially more seismicity than surrounding areas.

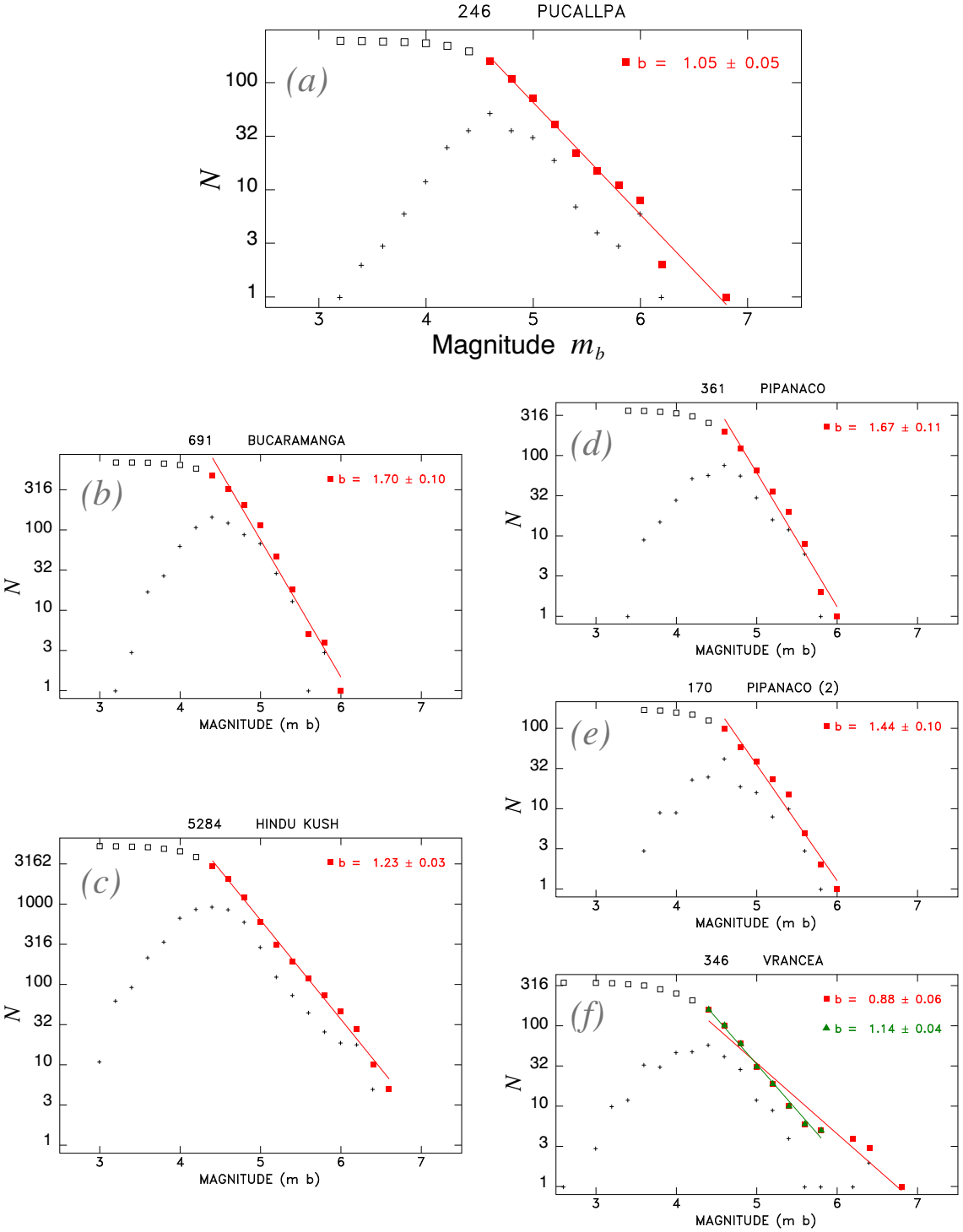

Fig. 5. Frequency-magnitude relationships for the Pucallpa (a), and other (b–f) seismic nests. In each frame, earthquakes from the NEIC 1963–2015 catalog are sorted by magnitude. The plus signs show the populations of the individual bins, of width 0.2 units of magnitude, and the squares represent the cumulative populations of events equal to, or greater than, a given magnitude. The regression is taken over the points highlighted in red, with the open symbols, affected by incompleteness, not used. In the case of Vrancea (f), a second regression is also shown in green that does not include the four largest earthquakes. While the horizontal axes (magnitude) are consistent for all plots, we note the different vertical axes for each plot required to show the significant variability in the absolute numbers of events. (For interpretation of the references to color in this figure legend, the reader is referred to the web version of this article.)

scale invariance and earthquake scaling laws, *b*-values are intrinsically controlled by the fractal dimension of the seismogenic zone. For earthquakes constrained to two-dimensional faults, the population of seismic moments is expected to feature a β value of 2/3 (obtained by regressing against $\log_{10} M_0$). If further assuming that a given magnitude grows as (2/3) $\log_{10} M_0$, a *b*-value of 1 is predicted for that magnitude scale. For a 3-dimensional seismogenic zone, as in the case of certain deep earthquakes (Okal and Kirby, 1995), β and *b* values are expected to be larger.

As discussed in detail by Okal and Romanowicz (1994), two effects conspire to produce systematic deviations to this model of constant *b*-value. One is physical, namely that in most geometries, the growth of

the fault width W is limited by the extent of the brittle material, leading to a breakdown in scaling laws, and to higher values for large events, even when studied as a function of moment. This effect is well known for major interplate earthquakes limited in width W by the thermal structure of the lithosphere, but on a smaller scale, it can express a limited length of coherence for faults, and predicts higher *b*-values in strongly heterogeneous, fractured media such as volcanic edifices. The second effect is the saturation of any magnitude measured at constant period (Kanamori and Anderson, 1975; Geller, 1976), which leads to additional curvature in the frequency-magnitude diagram, even before physical saturation of W can occur.

In the present context, and given the small number of available CMT solutions (except for the Hindu Kush nest), it is impossible to explore frequency-size relationships using the more analytical quantifier M_0, and we have to use the only magnitudes available, primarily m_b. The completeness of earthquake catalogues is of course a crucial element of any frequency-magnitude investigation. As discussed for example by Wiemer et al. (1998) and Wiemer and Wyss (2000), completeness may vary significantly, depending obviously on the level of instrumentation of a given province, but also on structural properties such as attenuation, not to mention a possible temporal variation, when the mechanism of seismogenesis can evolve, for example during a volcanic crisis (Wiemer et al., 1998). Wiemer and Wyss (2000) have based their estimates of completeness on the interpretation of the plateau developing in the cumulative populations used in *b*-value studies. In this regard, the datasets presented in Figs. 5 and 6 show clear breaks, especially when considering incremental bin populations (shown as + signs), which justify the magnitude ranges used in our investigations.

Our results show a regular value, $b = 1.05 \pm 0.05$, for the Pucallpa nest as a whole in the interval of probable completeness, $4.6 \leq m_b \leq 6.8$. This property is largely shared with the Vrancea nest ($b = 0.88$), in agreement with the previous models of Zarifi and Havskov (2003) and Prieto et al. (2012); note however a scatter at large magnitudes, and a slightly higher value ($b = 1.14$) when these events are excluded (Fig. 5f). The Hindu Kush nest is the only one for which a moment regression is possible, yielding $\beta = 0.60 \pm 0.03$, in reasonable agreement with the theoretical value 2/3; by contrast, $b = 1.23$ reflects the initiation of saturation for a population featuring a consequent number of events with $m_b > 6$. In the case of Bucaramanga, we obtain a high *b*-value (1.70), which agrees with Prieto et al.'s (2012) (however, they guard against the use of particular sets of magnitudes, i.e. m_b vs. M_L), and Frohlich and Nakamura's (2009); we note a possible change of slope around $m_b = 5$. Finally, we find relatively high values for the Pipanaco events, especially when considering the full nest.

While the Pucallpa nest features *b*-values essentially equal to 1 (an attribute it shares with Vrancea, and which agrees well, within the range of magnitudes considered that are little affected by saturation, with the β value (0.70) documented by Okal and Kirby (1995) in the 100–200 km depth band), we note that the two legs of the Pucallpa nest have distinctly different b-values when considered independently. The WSW trending southern leg that is aligned with the MFZ has a higher b-value (1.29 ± 0.08) than the NNW trending leg (0.90 ± 0.05) (top frames of Fig. 6). This difference could reflect differences in the coherence of faults within the oceanic plate associated with the two legs. The more fractured oceanic crust of the MFZ might be expected to produce more smaller earthquakes than the less fractured rock associated with the NNW trending leg, whose *b*-value (0.90) is essentially identical to that of the Vrancea nest (0.88). This difference appears robust with respect to the details governing the separation of the two legs of the nest: on the bottom frames of Fig. 6, we assign the events in the heel of the nest to the Southern rather than Northern leg, with essentially no effect on the resulting *b*-values, the new ones remaining within the error bars of the top frames.

2.2. Focal mechanisms

The focal mechanisms for events within the Pucallpa nest indicate nearly exclusively normal faulting geometries in map view. Fig. 7 shows focal mechanisms available in the Global CMT catalog (Dziewonski et al., 1981; Ekström et al., 2012) for earthquakes larger than magnitude 5.5 between 1990 and 2015. For the NNW-SSE trending long leg of the nest, almost all focal mechanisms have one sub-horizontal nodal plane and one near vertical nodal plane aligned roughly parallel to the trench. In cross section (Fig. 7A), these focal mechanisms are all consistent with downdip extension within the slab east of the horizontal slab segment. For the WSW-trending shorter leg, the focal mechanisms are more variable. While the P-axes are relatively consistently near vertical, there is significant scatter in the orientation of the T-axes.

The consistency of focal mechanisms in the Pucallpa nest can be quantified by first summing (without weighting) the moment tensors of the available solutions and defining a resulting "average" best double-couple ($\phi = 343^\circ$; $\delta = 73^\circ$; $\lambda = -100^\circ$; with a minimal minor double-couple of only 3%). We then compute, for each solution, the angle of solid rotation separating it from that average, in the formalism of Kagan (1991). We find that the Kagan angles are generally $< 30^\circ$ (out of a theoretical maximum of 120°), and with one exception (57°) $< 40^\circ$, the angles being particularly low in the Northern leg of the "L", thus confirming the coherence in the focal geometries.

3. The Pucallpa Nest and its location in the Peruvian Flat slab

A number of models for the geometry of the Nazca Plate that are based on teleseismic locations of slab seismicity have noted the presence of a broad flat slab that extends for most of the Peruvian margin. Cahill and Isacks (1992) envisioned this slab as a uniform bench-like structure with little along-strike variability in depth or trench-perpendicular extent. Others like Gutscher et al. (1999) and more recently Slab 2.0 (Hayes et al., 2018) indicate that there may be significant along-strike changes in the shape of the downgoing plate within the flat slab region. Gutscher et al. (1999) in particular advocated for a sag in the Nazca plate between the fully subducted Inca Plateau and the downgoing Nazca Ridge (Figs. 2, 7). Supporting evidence for such a sag, at least to the south, was later confirmed by the Peru Lithosphere and Slab Experiment (PULSE; Wagner et al., 2010) by means of a variety of analyses including earthquake locations (Kumar et al., 2016), surface wave tomography (Antonijevic et al., 2015, 2016) and receiver functions (Bishop et al., 2017). However, the northward extent of the sag is less well constrained.

The location of the Pucallpa nest shown in this study strongly suggests that these earthquakes lie just north of the sag, as opposed to within the sag as proposed by Gutscher et al. (1999). While the Pucallpa nest is clearly visible in Fig. 2a and b of Gutscher et al. (1999), they are projected to the east a significant distance, masking the fact that many of the events, especially in the NNW trending leg, lie within the downgoing portion of the Nazca plate, beyond the flat slab. The shallowest events of this cluster, however, are at approximately the same depth as those proposed to be co-located with the subducted Inca Plateau to the north, consistent with them being located north of the sag and not within it.

Some clues on the relationship between the Pucallpa nest and the flat slab sag can be gleaned from comparing the Pucallpa nest focal mechanisms with those of the Bucaramanga and Pipanaco nests. For Bucaramanga and Pipanaco, the T-axis orientations are dominantly parallel to the slab, pointing in the downdip direction. For the Bucaramanga nest, we document significant diversity in focal mechanisms, with the 35 available GCMT solutions deviating 53° in mean Kagan angle from their average best double-couple, a conclusion in line with previous studies (e.g. Schneider et al., 1987). However, most focal mechanisms feature slab-downdip extension with variable orientations of the other two axes (e.g. Frohlich et al., 1995; Cortés and Angelier,

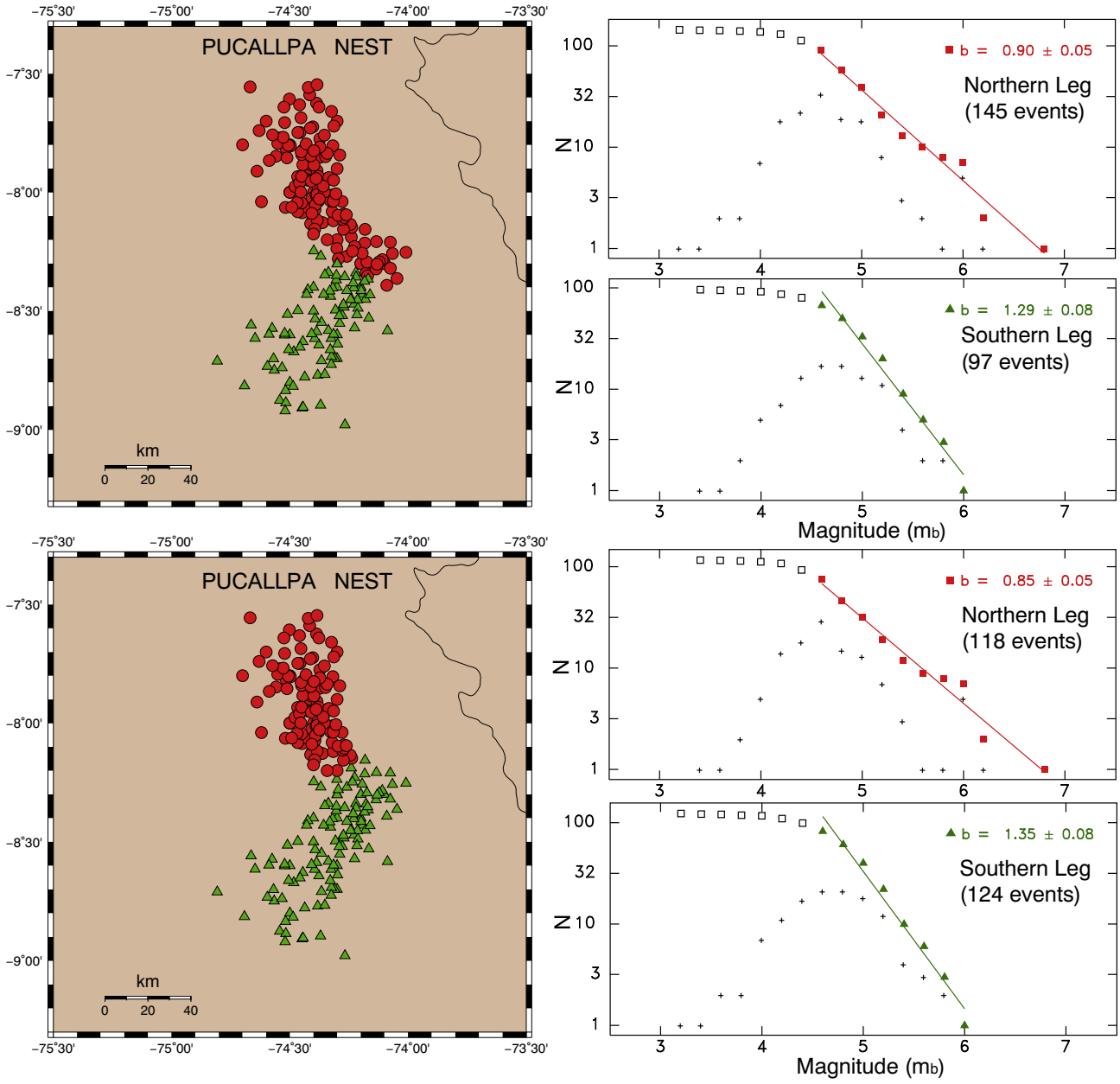

Fig. 6. Frequency-magnitude relationship of Pucallpa nest legs. *b*-Value results obtained by splitting the Pucallpa nest into its NNW-trending and WSW-trending legs (red circles and green triangles respectively on maps). Note significantly different slopes, compatible with a more fractured material under the WSW-trending group. Comparison between the top and bottom frames, which differ in the assignment of events at the intersection of the legs, demonstrates the robustness of this result. (For interpretation of the references to color in this figure legend, the reader is referred to the web version of this article.)

2005; Prieto et al., 2012). For the Pipanaco nest, revised slab contours based on improved earthquake locations also indicate consistently downdip T-axis orientations (Mulcahy et al., 2014). In the Pucallpa nest, the NNW trending limb shows a similar pattern to Bucaramanga and Pipanaco: consistently downdip extensional focal mechanisms. However, the WSW trending limb indicates a greater degree of variability in T-axis orientation. This may simply reflect an absence of a dominant downdip direction in a portion of the flat slab with only gradually changing dip direction. Alternatively, this heterogeneity may be due to either abrupt changes in slab geometry and therefore in downdip slab direction, or it may be due to differing styles of slab deformation.

The slab deformation associated with the Bucaramanga nest events has been attributed to slab pull, slab bending, slab tearing, and/or the collision between two subducting plates (e.g. Frohlich et al., 1995; Taboada et al., 2000; Cortés and Angelier, 2005; Zarifi et al., 2007; Syracuse et al., 2016). For Pipanaco, Mulcahy et al. (2014) propose a much more abrupt transition from flat slab to normally dipping slab in the region of the Pipanaco nest than had previously been reported, and suggest that this additional degree of deformation and associated extension may play a role in the genesis of the nest seismicity. We postulate that the NNW leg of the Pucallpa nest is due to slab pull/downdip extension. Another possibility is that this leg of the Pucallpa nest is due to slab bending forces. Slab bending has been postulated to play a significant role in the development of intermediate depth seismicity (e.g. Faccenda et al., 2012). Indeed, the damaging 2017 M_w7.1 Puebla-Morelos earthquake was located at the northernmost margin of the Mexican flat slab, and has been postulated to be caused by a bending-related reactivation of pre-existing faults in the subducted plate (Melgar et al., 2018). However, we note that the near vertical trend of this leg of

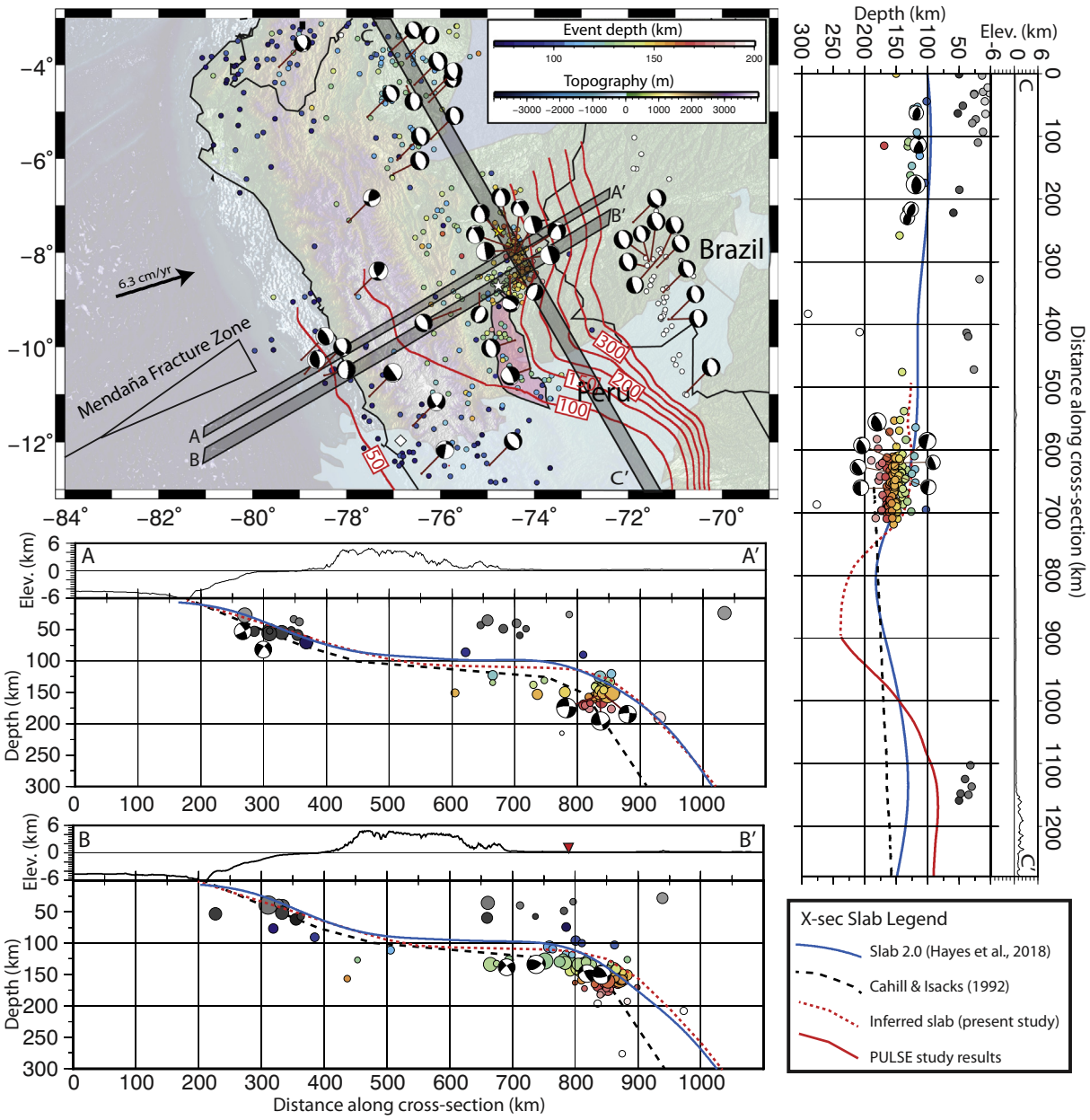

Fig. 7. Map of Pucallpa Nest with focal mechanisms and cross sections. Top: map view: circles show seismicity (same as Fig. 2) along with focal mechanisms from the Global CMT catalog (Dziewonski et al., 1981; Ekström et al., 2012). The red contours are our proposed slab geometry in 50 km increments. Teal outlined shape is the projected location of the subducted Nazca Ridge based on its conjugate Tuamotu Plateau on the Pacific plate (Hampel, 2002). The dark blue outlined shape is the subducted Inca Plateau based on the location of its conjugate, the Marquesas Plateau (Rosenbaum et al., 2005). The pink shaded region shows the location of the Shira Mountains (Hermoza et al., 2006). Cross sections have earthquakes and focal mechanisms projected onto the transect from within the boxes outlined on the map. For all cross sections, the red line is the proposed slab geometry shown in red contours and in Fig. 7 – the solid red line indicates the slab geometry determined from PULSE studies (e.g. Antonijevic et al., 2015, 2016; Kumar et al., 2016; Bishop et al., 2017) and the dashed red line indicates the slab geometry inferred in the present study. The dashed black line is the slab from Cahill and Isacks (1992). The blue line is the slab from Slab2.0 (Hayes et al., 2018). The black line above the depth profiles on each cross section shows topography/bathymetry in km. Middle: Cross-section A–A′ through the NNW-SSE trending arm of the Pucallpa Nest. T-axes are uniformly down-dip, roughly parallel to the dip of the proposed slab geometry. Bottom: Cross-section B–B′ is parallel to the WSW-ENE arm of the Pucallpa Nest. Focal mechanisms on this segment are more variable. The inverted red triangle on the topography profile shows the location of the Agua Caliente Oil Field and Boiling River. Cross-section C–C′ is parallel to the NNW-SSE arm of the Pucallpa Nest. (For interpretation of the references to color in this figure legend, the reader is referred to the web version of this article.)

the nest extends over 40 km depth with little apparent variation in available focal mechanisms. If all of these events are associated with the bending of the plate, one might expect a range in mechanisms from extensional at the top of the plate to compressional at the bottom. Given the limited number of focal mechanisms available, we cannot rule out this possibility without further study. Furthermore, any such study would also need to explain why this leg of the Pucallpa nest does not extend further to the north or south. Possible explanations could include variability in the slab geometry which is poorly constrained to the north, or the absence of favorably oriented subducted plate fabric (Melgar et al., 2018).

The WSW leg of the Pucallpa nest on the other hand, appears to lie along the northern edge to the sag between the northern and southern segments of the Peruvian flat slab. The abruptness of this transition to

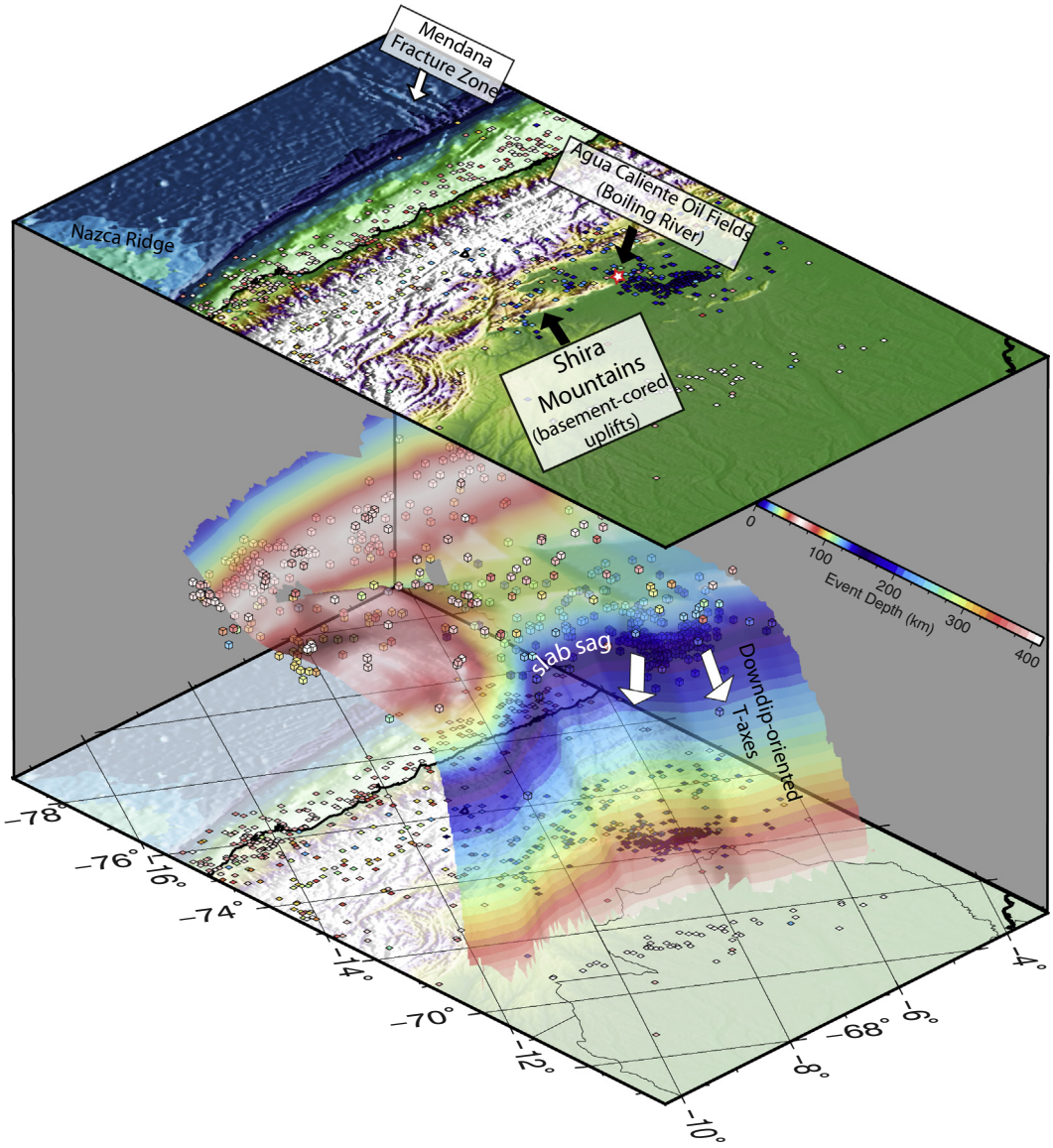

Fig. 8. 3D image of slab seismicity and possible slab geometry surrounding the Pucallpa Nest. Cubes show event location for seismicity > 70 km depth from the RISC 1990–2015. Squares on underlying and overlying topographic maps show projections of the same events. Slab geometry south of ~9°S is constrained by seismic stations of the PULSE deployment (see Fig. 2). Slab geometry proposed here for areas further north is based on RISC event locations and focal mechanisms.

the sag is difficult to discern from earthquake locations alone. However, given the orientations of the focal mechanisms along the WSW leg of the Pucallpa nest, we postulate that this may be a relatively abrupt transition that could be accommodated by bending and/or extension as suggested for both the Bucaramanga and Pipanaco nests, or by slab tearing as has been suggested for Bucaramanga.

The WSW leg of the Pucallpa nest is oriented roughly parallel to the downgoing MFZ. The MFZ is a broad region (80 km) of trench-perpendicular lineations (Kukowski et al., 2008) once thought to comprise a young (< 3.5 Ma) active spreading center (Huchon and Bourgois, 1990) but now thought to be a complex segmented transform fault (Lonsdale, 2005) that separates 27–30 Ma oceanic crust to the north from 36 to 41 Ma to the south (Müller et al., 2008). The alignment of the WSW arm of the Pucallpa nest with the MFZ and possibly with an abrupt deepening of the slab to the south of the MFZ is consistent both with the MFZ being a zone of weakness that might accommodate either abrupt slab deformation and/or tearing, and with the oceanic plate being older, and therefore colder and more dense to the south of the MFZ than to the north. This is also consistent with the higher b-values obtained for this leg of the Pucallpa nest that may indicate the presence of more fractured oceanic plate.

Fig. 8 shows a 3D representation of our proposed slab geometry, along with seismicity, topography, and other geological features. Several surface geologic features correlate spatially and temporally with the sag and the development of the flat slab, respectively. The Shira uplift is a late Miocene-to-recent basement cored uplift that separates the Pachitea Basin to the west from the Ucayali Basin further east (Hermoza et al., 2006; Espurt et al., 2008; Devlin et al., 2012; Gautheron et al., 2013; Witte et al., 2015). The timing of this uplift (9 ± 2 Ma) is similar to the beginning of the subduction of the Nazca Ridge and associated formation of the flat slab at these latitudes (Rosenbaum et al., 2005; Gautheron et al., 2013). The inverted Paleozoic faults that define the eastern margin of the Shira Mountains appear to lie near the downward inflection point of the sagging portion of the Peruvian flat slab. The along-strike extent of the Shira Mountains correlates well with the along-strike extent of the sag. However, correlation does not mean causation. The nature of a causal relationship (if one exists) between flat slabs and basement cored uplifts is not well

understood or agreed upon even in well instrumented regions, and is therefore well beyond the scope of the present study. However, we propose that this region may provide valuable constraints on this relationship due to the along-strike variability in both slab geometry and overriding deformation.

4. Conclusions

1) The Pucallpa Nest in central Peru meets all of the criteria for a seismic nest, bringing to three the number of seismic nests associated with flat slabs in South America. Its spatial correlation with the Mendaña fracture zone and its similarity to other flat slab seismic nests may provide new constraints on the causes of intermediate depth seismicity (e.g. Prieto et al., 2012).
2) The two legs of the Pucallpa Nest are characterized by differences in both focal mechanisms and b-values. The NNW trending leg is characterized by very consistent focal mechanisms and average-to-low b-values. The WSW trending leg of the nest has significantly more variability in focal mechanisms, and has a relatively high b-value. This may reflect the role of the Mendaña fracture zone in the genesis of this portion of the seismic nest.
3) The WSW leg of the Pucallpa Nest and associated Mendaña fracture zone appears to define the northern margin of a sag in the Peruvian flat slab. The sag may therefore be due, in part, to the presence of 10 Ma older oceanic plate to the south of the fracture zone than to the north. The fracture zone itself may form a zone of weakness that allows for both the seismicity of the Pucallpa Nest and also the bending or tearing required to produce this sag.
4) The geometry of the Peruvian flat slab correlates well spatially with the location of the basement cored uplifts of the Shira Mountains, both in along-strike extent and its location above the eastern hinge of the flat slab. More work is needed to understand the causes of flat slab nests and the role they play in the spatio-temporal evolution of slab geometry.

Acknowledgements

We would like to thank Diana Roman for thoughtful ongoing conversations about the Pucallpa Nest and its tectonic implications. The southern Peruvian flat slab geometry would not have been possible without the contributions of students and collaborators on the PULSE seismic deployment (NSF-Geophysics EAR-044184 (LSW)), especially Susan Beck, Maureen Long, Hernando Tavera, and Cristobal Condori. We would like to thank Shawn Wei and two other anonymous reviewers for helpful comments and suggestions that improved the clarity of this manuscript.

References

Altamimi, Z., Rebishung, P., Métivier, L., Collilieux, X., 2016. A new release of the International Terrestrial Reference Frame modeling nonlinear station motions. J. Geophys. Res. 121 (8), 6109–6131. https://doi.org/10.1002/2016JB013098.

Alvarez, J.O.S., 2008. Structural and Stratigraphic Evolution of Shira Mountains, Central Ucayali Basin, Perú. Doctoral dissertation. Texas A & M University.

Anderson, M., Alvarado, P., Zandt, G., Beck, S., 2007. Geometry and brittle deformation of the subducting Nazca Plate, Central Chile and Argentina. Geophys. J. Int. 171 (1), 419–434.

Antonijevic, S.K., Wagner, L.S., Kumar, A., Beck, S.L., Long, M.D., Zandt, G., Tavera, H., Condori, C., 2015. The role of ridges in the formation and longevity of flat slabs. Nature 524, 212–215.

Antonijevic, S.K., Wagner, L.S., Beck, S.L., Long, M.D., Zandt, G., Tavera, H., 2016. Effects of change in slab geometry on the mantle flow and slab fabric in Southern Peru. Journal of Geophysical Research: Solid Earth 121 (10), 7252–7270.

Bishop, B., Beck, S.L., Zandt, G., Wagner, L.S., Long, M.D., Antonijevic, S.K., Kumar, A., Tavera, H., 2017. Causes and consequences of flat-slab subduction in southern Peru. Geosphere, v 13 (5), 1392–1407. https://doi.org/10.1130/GES01330.1.

Cahill, T., Isacks, B.L., 1992. Seismicity and shape of the subducted Nazca plate. J. Geophys. Res. 97, 17503–17529.

Chang, Y., Warren, L.M., Prieto, G.A., 2017. Precise locations for intermediate-depth earthquakes in the Cauca Cluster, Colombia. Bull. Seis. Soc. Am 107, 2649–2663.

Chen, P.-F., Nettles, M., Okal, E.A., Ekström, G., 2001. Centroid Moment Tensor solutions for intermediate-depth earthquakes of the WWSSN-HGLP era (1962–1975). Phys. Earth Planet. Inter. 124, 1–7.

Cortés, M., Angelier, J., 2005. Current states of stress in the northern Andes as indicated by focal mechanisms of earthquakes. Tectonophysics 403 (1–4), 29–58.

Devlin, S., Isacks, B.L., Pritchard, M.E., Barhart, W.D., Lohman, R.B., 2012. Depths and focal mechanisms of crustal earthquakes in the central Andes determined from teleseismic waveform analysis and InSAR. Tectonics 31. https://doi.org/10.1029/2011TC002914.

Dziewonski, A.M., Chou, T.-A., Woodhouse, J.H., 1981. Determination of earthquake source parameters from waveform data for studies of global and regional seismicity. J. Geophys. Res. 86, 2825–2852. https://doi.org/10.1029/JB086iB04p02825.

Ekström, G., Nettles, M., Dziewonski, A.M., 2012. The global CMT project 2004–2010: centroid-moment tensors for 13,017 earthquakes. Phys. Earth Planet. Inter. 200-201 (1–9), 2012. https://doi.org/10.1016/j.pepi.2012.04.002.

Espurt, N., Brusset, S., Baby, P., Hermoza, W., Bolaños, R., Uyen, D., Déramond, J., 2008. Paleozoic structural controls on shortening transfer in the Subandean foreland thrust system, Ene and southern Ucayali basins, Peru. Tectonics 27 (3). https://doi.org/10.1029/2007TC002238.

Faccenda, M., Gerya, T.V., Mancktelow, N.S., Moresi, L., 2012. Fluid flow during slab unbending and dehydration: implications for intermediate-depth seismicity, slab weakening and deep water recycling. Geochem. Geophys. Geosyst. 13 (1). https://doi.org/10.1029/2011GC003860.

Frohlich, C., Nakamura, Y., 2009. The physical mechanism of deep moonquakes and intermediate-depth earthquakes: how similar and how different? Phys. Earth Plan. Inter 173, 365–374.

Frohlich, C., Kadinsky-Cade, K., Davis, S.D., 1995. A re-examination of the Bucaramanga, Colombia, Earthquake Nest. Bull. Seis. Soc. Am. 85 (6), 1622–1634.

Gautheron, C., Espurt, N., Barbarand, J., Roddaz, M., Baby, P., Brusset, S., Tassan-Got, L., Douville, E., 2013. Direct dating of thick-and thin-skin thrusts in the Peruvian Subandean zone through apatite (U–Th)/He and fission track thermochronometry. Basin Res. 25 (4), 419–435.

Geller, R.J., 1976. Scaling relations for earthquake source parameters and magnitudes. Bull. Seismol. Soc. Am. 66, 1501–1523.

Georgescu, E.S., 2002. The partial collapse of Coltzea Tower during the Vrancea earthquake of 14/26 October 1802: the historical warning of long-period ground motion site effects in Bucharest. In: Proc. Intl. Conf. Earthq. Loss Estim. Risk Reduction, Bucharest.

Gerya, T.V., Fossati, D., Cantieni, C., Seward, D., 2009. Dynamic effects of aseismic ridge subduction: numerical modelling. Eur. J. Mineral. 21 (3), 649–661.

Global Volcanism Program, 2013. In: Venzke, E. (Ed.), Volcanoes of the World, v. 4.7.1. Smithsonian Institution. https://doi.org/10.5479/si.GVP.VOTW4-2013. Downloaded 3 Jul 2018.

Green, H.W., Houston, H., 1995. The mechanics of deep earthquakes. Annu. Rev. Earth Planet. Sci. 23 (1), 169–213.

Gutscher, M.A., Olivet, J.L., Aslanian, D., Eissen, J.P., Maury, R., 1999. The "lost Inca Plateau": cause of flat subduction beneath Peru? Earth Planet. Sci. Lett. 171 (3), 335–341.

Gutscher, M.A., Spakman, W., Bijwaard, H., Engdahl, E.R., 2000. Geodynamics of flat subduction: seismicity and tomographic constraints from the Andean margin. Tectonics 19 (5), 814–833.

Hacker, B.R., Peacock, S.M., Abers, G.A., Holloway, S.D., 2003. Subduction factory 2. Are intermediate-depth earthquakes in subducting slabs linked to metamorphic dehydration reactions? Journal of Geophysical Research: Solid Earth 108 (B1), 2030. https://doi.org/10.1029/2001JB001129.

Hampel, A., 2002. The migration history of the Nazca Ridge along the Peruvian active margin: a re-evaluation. Earth Planet. Sci. Lett. 203 (2), 665–679.

Hayes, G.P., Moore, G.L., Portner, D.E., Mearne, M., Flamme, H., Furtney, M., Smoczyk, G.M., 2018. Slab2, a comprehensive subduction zone geometry model. Science. https://doi.org/10.1126/science.aat4723.

Hermoza, W., Baby, P., Espurt, N., Martinez, E., Bolaños, R., 2006. The Ucayali Subandean basin: a complex fold and thrust belt and inverted system. In: IX Simposio Bolivariano, Petroleum Exploration in the Subandean Basins; Cartagena de las Indias, Sept 2006, Cartagena, Colombia.

Huchon, P., Bourgois, J., 1990. Subduction-induced fragmentation of the Nazca plate off Peru: Mendaña fracture zone and Trujillo Trough revisited. J. Geophys. Res. 95 (B6), 8419–8436.

International Seismological Centre, 2015. On-line Bulletin. http://www.isc.ac.ukInternatl. Seismol. Cent, Thatcham, United Kingdom.

Isacks, B.L., Sykes, L.R., Oliver, J., 1967. Spatial and temporal clustering of deep and shallow earthquakes in the Fiji-Tonga-Kermadec region. Bull. Seis. Soc. Am. 57, 935–958.

James, D.E., Snoke, J.A., 1994. Structure and tectonics in the region of flat subduction beneath central Peru: crust and uppermost mantle. J. Geophys. Res. 99 (B4), 6899–6912.

John, T., Medvedev, S., Rüpke, L.H., Andersen, T.B., Podladchikov, Y.Y., Austrheim, H., 2009. Generation of intermediate-depth earthquakes by self-localizing thermal runaway. Nat. Geosci. 2 (2), 137.

Kagan, Y.Y., 1991. 3-D rotation of double-couple earthquake sources. Geophys. J. Intl 106, 709–716.

Kanamori, H., Anderson, D.L., 1975. Theoretical basis of some empirical relations in seismology. Bull. Seismol. Soc. Am. 65, 1073–1095.

Kay, S.M., Mpodozis, C., 2001. Central Andean ore deposits linked to evolving shallow subduction systems and thickening crust. Geological Society of America Today 11, 4–9.

Kelemen, P.B., Hirth, G., 2007. A periodic shear-heating mechanism for intermediate-depth earthquakes in the mantle. Nature 446 (7137), 787.

Kirby, S.H., Stein, S., Okal, E.A., Rubie, D., 1996. Deep earthquakes and metastable mantle phase transformations in subducting oceanic lithosphere. Revs. Geophys. Space Phys., v. 34, 261–306.
Kukowski, N., Hampel, A., Hoth, S., Bialas, J., 2008. Morphotectonic and morphometric analysis of the Nazca plate and the adjacent offshore Peruvian continental slope—implications for submarine landscape evolution. Mar. Geol. 254 (1–2), 107–120.
Kumar, A., Wagner, L.S., Beck, S.L., Long, M.D., Zandt, G., Young, B., Tavera, H., Minaya, E., 2016. Seismicity and state of stress in the central and southern Peruvian flat slab. Earth Planet. Sci. Lett. 441, 71–80.
Lonsdale, P., 2005. Creation of the Cocos and Nazca plates by fission of the Farallon plate. Tectonophysics 404 (3), 237–264.
Manea, V.C., Pérez-Gussinyé, M., Manea, M., 2012. Chilean flat slab subduction controlled by overriding plate thickness and trench rollback. Geology 40 (1), 35–38.
Melgar, D., Pérez-Campos, X., Ramirez-Guzman, L., Spica, Z., Espíndola, V.H., Hammond, W.C., Cabral-Cano, E., 2018. Bend faulting at the edge of a flat slab: the 2017 Mw7. 1 Puebla-Morelos, Mexico earthquake. Geophys. Res. Lett. 45 (6), 2633–2641.
Mulcahy, P., Chen, C., Kay, S.M., Brown, L.D., Isacks, B.L., Sandvol, E., Heit, B., Yuan, X., Coira, B.L., 2014. Central Andean mantle and crustal seismicity beneath the Southern Puna plateau and the northern margin of the Chilean-Pampean flat slab. Tectonics 33, 1636–1658. https://doi.org/10.1102/2013TC003393.
Müller, R.D., Sdrolias, M., Gaina, C., Roest, W.R., 2008. Age, spreading rates, and spreading asymmetry of the world's ocean crust. Geochem. Geophys. Geosyst. 9 (4). https://doi.org/10.1029/2007GC001743.
Navarro Comet, J., 2018. The Agua Caliente oilfield and the boiling river of the Peruvian Amazon. AAPG Explorer 39 (3), 20–25.
Newman, A.V., Okal, E.A., 1998. Teleseismic estimates of radiated seismic energy: the E/M_0 discriminant for tsunami earthquakes. J. Geophys. Res. 103, 26885–26898.
O'Driscoll, L.J., Richards, M.A., Humphreys, E.D., 2012. Nazca–South America interactions and the late Eocene–late Oligocene flat-slab episode in the central Andes. Tectonics 31 (2).
Okal, E.A., Kirby, S.H., 1995. Frequency-moment distribution of deep earthquakes: implications for the seismogenic zone at the bottom of slabs. Phys. Earth Planet. Inter 92, 169–187.
Okal, E.A., Romanowicz, B.A., 1994. On the variation of *b*-value with earthquake size. Phys. Earth Planet. Inter 87, 55–76.
Okazaki, K., Hirth, G., 2016. Dehydration of lawsonite could directly trigger earthquakes in subducting oceanic crust. Nature 530 (7588), 81.
Poli, P., Prieto, G., Rivera, E., Ruiz, S., 2016. Earthquakes initiation and thermal shear instability in the Hindu Kush intermediate depth nest. Geophys. Res. Lett. 43 (4), 1537–1542.
Prieto, G.A., Beroza, G.C., Barrett, S.A., Lopez, G.A., Florez, M., 2012. Earthquake nests as natural laboratories for the study of intermediate-depth earthquake mechanics. Tectonophysics 570-571, 42–56.
Prieto, G.A., Florez, M., Barrett, S.A., Beroza, G.C., Pedraza, P., Blanco, J.F., Poveda, E., 2013. Seismic evidence for thermal runaway during intermediate-depth earthquake rupture. Geophys. Res. Lett. 40 (23), 6064–6068.
Rosenbaum, G., Giles, D., Saxon, M., Betts, P.G., Weinberg, R.F., Duboz, C., 2005. Subduction of the Nazca Ridge and the Inca Plateau: insights into the formation of ore deposits in Peru. Earth Planet. Sci. Lett. 239 (1–2), 18–32.
Rundle, J.B., 1989. Derivation of the complete Gutenberg-Richter magnitude-frequency relation using the principle of scale invariance. J. Geophys. Res. 94, 12337–12342.
Ruzo, A., 2016. The Boiling River. Simon and Schuster, New York, NY.
Sacks, I.S., Suyehiro, S., Kamitsuki, A., Tuve, M.A., Otsuka, M., Saa, G., Rodriguez, A., Gajardo, E., Cabre, R., Fernandeza, L., Volponi, F., Giesecke, A., Aldrich, L.T., 1966. A tentative value of Poisson's coefficient from the seismic “Nest of Socompa”. Annual Report of the Director, Carnegie Institution of Washington Department of Terrestrial Magnetism 1965-1966, 43–45.
Saloor, N., Okal, E.A., 2018. Extension of the energy-to-moment parameter Θ to intermediate and deep earthquakes. Phys. Earth Planet. Inter 274, 37–48.
Schneider, J.F., Pennington, W.D., Meyer, R.P., 1987. Microseismicity and focal mechanisms of the intermediate-depth Bucaramanga Nest, Colombia. J. Geophys. Res. 92 (B13), 13913–13926.
Scire, A., Zandt, G., Beck, S.L., Long, M.D., Wagner, L.S., Minaya, E., Tavera, H., 2016. Imaging the transition from flat to normal subduction: variations in the structure of the Nazca slab and upper mantle under southern Peru and northwestern Bolivia. Geophys. J. Int. 204, 457–479.
Shuler, A., Ekström, G., Nettles, M., 2013. Physical mechanisms for vertical-CLVD earthquakes at active volcanoes. Journal of Geophysical Research: Solid Earth 118, 1569 – 1586.
Syracuse, E.M., Maceira, M., Prieto, G.A., Zhang, H., Ammon, C.J., 2016. Multiple plates subducting beneath Colombia, as illuminated by seismicity and velocity from the joint inversion of seismic and gravity data. Earth Planet. Sci. Lett. 444, 139–149.
Taboada, A., Rivera, L.A., Fuenzalida, A., Cisternas, A., Philip, H., Bijwaard, H., Olaya, J., Rivera, C., 2000. Geodynamics of the northern Andes: subductions and intracontinental deformation (Colombia). Tectonics 19 (5), 787–813.
Tavera, H., 2012. A report on the 24 August 2011 M_w 7.0 Contamana, Peru, Intermediate-depth earthquake. Seis. Res. Lett 83 (6), 1007–1013.
Wagner, L., Beck, S.L., Long, M.D., 2010. PerU Lithosphere and Slab Experiment. International Federation of Digital Seismograph Networks, Other/Seismic Network. https://doi.org/10.7914/SN/ZD_2010.
Wiemer, S., Wyss, M., 2000. Minimum magnitude of completeness in earthquake catalogs: examples form Alaska, the Western United States and Japan. Bull. Seismol. Soc. Am. 90, 859 – 869.
Wiemer, S., McNutt, S.R., Wyss, M., 1998. Temporal and three-dimensional spatial analysis of the frequency-magnitude distribution near Long Valley caldera, California. Geophys. J. Intl 134, 409 – 421.
Witte, J., Rebaza, J., Westlund, D., Stratton, M., Alegria, C., 2015. A new structural model of the Pachitea Basin, Peru: interaction of thick-skinned tectonics and salt detached thrusting. J. S. Am. Earth Sci. 63, 400–416.
Yáñez, G.A., Ranero, C.R., von Huene, R., Díaz, J., 2001. Magnetic anomaly interpretation across the southern central Andes (32–34 S): the role of the Juan Fernández Ridge in the late Tertiary evolution of the margin. Journal of Geophysical Research: Solid Earth 106 (B4), 6325–6345.
Zarifi, Z., Havskov, J., 2003. Characteristics of dense nests of deep and intermediate-depth seismicity. Adv. Geophys. 46, 237–278.
Zarifi, Z., Havskov, J., Hanyga, A., 2007. An insight into the Bucaramanga nest. Tectonophysics 443, 93–105.